Development of a fourfold dielectric-filled reentrant cavity as a beam position monitor (BPM) in a proton therapy facility

Srinivasan, S.; Brandenburg, S.; Schippers, J. M.; Duperrex, P. A.

Published in:
Journal of Instrumentation

DOI:
10.1088/1748-0221/17/09/P09013

Published by IOP Publishing for Sissa Medialab
Received: *January 20, 2022*
Revised: *June 22, 2022*
Accepted: *August 10, 2022*
Published: *September 12, 2022*

Development of a fourfold dielectric-filled reentrant cavity as a beam position monitor (BPM) in a proton therapy facility

S. Srinivasan,[a,b,*] **S. Brandenburg,**[c,d] **J.M. Schippers**[a,d] **and P.A. Duperrex**[a]

[a] *Paul Scherrer Institute (PSI),*
Forschungsstrasse 111, 5232, Villigen, Switzerland
[b] *Bergoz Instrumentation,*
56 Rue du Mont Rond, 01630, Saint-Genis-Pouilly, France [1]
[c] *KVI-Center for Advanced Radiation Technology, University of Groningen,*
Zernikelaan 25, 9747 AA, Groningen, The Netherlands
[d] *Department of Radiation Oncology, University Medical Center Groningen, University of Groningen,*
9713 GZ, Groningen, The Netherlands

E-mail: sudharsan.srinivasan@psi.ch

Abstract: At the Paul Scherrer Institute (PSI), the superconducting cyclotron "COMET" delivers a 250 MeV proton beam for radiation therapy in pulses of 1ns at the cyclotron-RF frequency of 72.85 MHz. Accurate measurement of the beam position at proton beam currents of 0.1–10 nA in the beam transport line downstream of the degrader is of crucial importance for the treatment safety and quality, beam alignment and feedback systems. This is essential for efficient operation and beam delivery. These measurements are usually performed with intercepting monitors such as ionization chambers (ICs). In this paper, we present a novel non-intercepting position sensitive cavity resonator. The resonant monitor, tuned to the second harmonic of the cyclotron's RF, is based on the detection of the transverse magnetic dipole mode of the EM field generated by the beam. This mode is only excited for off-center beam positions and is measured with the help of four floating cavities within a common grounded cylinder. This paper discusses the BPM fundamental characteristics, design optimization and the underlying parametric investigations involving the contribution of the different modes and crosstalk. We estimate the expected signals from the prototype BPM for position offsets from simulations and compare them with test-bench measurements and beam measurements with the prototype and the improvised BPM design. We conclude by summarizing the achieved position sensitivity, precision, and measurement bandwidth.

Keywords: Beam-line instrumentation (beam position and profile monitors, beam-intensity monitors, bunch length monitors); Instrumentation for hadron therapy; Instrumentation for particle-beam therapy; Models and simulations

*Corresponding author.
[1] Current affiliation.

https://doi.org/10.1088/1748-0221/17/09/P09013

2022 JINST 17 P09013

Contents

1 Introduction

The proton therapy facility at PSI, PROSCAN [1], uses a superconducting isochronous cyclotron, COMET, in which the protons are accelerated to 250 MeV with an RF frequency of 72.85 MHz, which is also the repetition rate of the extracted proton bunches. The beam from COMET is sent through a degrader for energy modulation in the range 238–70 MeV. The beam parameters are summarized in table 1.

After the degrader, the beam is transported to one of the three gantries or to a beamline specifically for eye tumor irradiations. To comply with the safety and reliability requirements for operation, multiple checkpoints have been incorporated to measure beam parameters such as current, position, energy etc. This set of information is obtained using dedicated beam monitoring systems [2], that are mostly of interceptive nature. The choice of having ICs permanently inserted in the beamline is a decision made in the design phase of the PSI facility. Most of the clinically operating facilities don't possess such interceptive diagnostic devices in their beam transport sections to minimize investment costs and maintenance costs that involve frequent replacement due to sputtering damage. The interceptive beam diagnostics are placed at the cyclotron exit and in the nozzle.

2022 JINST 17 P09013

Table 1. Extracted beam from the COMET cyclotron and its properties.

Beam Properties	Units
Extracted beam current	<1–800 nA
Energy spread ΔE/E at extraction	0.15%
ΔE/E Beyond the degrader and energy selection system	0.2% at 230 MeV; 2.5% at 70 MeV
Beam current beyond degrader and energy selection system	0.1–10 nA
Beam diameter	1–20 mm
Bunch repetition rate (= RF frequency)	72.85 MHz (T = 13.73 ns)
Micro bunch length and charge at degrader exit for all energies	2 ns; ≈0.01 fC (for 1 nA average current)

At several locations in the beam lines of PROSCAN, beam position and beam current are measured to ensure that the beam transport is as expected and to supervise the maximum beam current that can be allowed on the gantry during the standard patient treatment [3, 4]. This is intended to prevent delivery errors i.e., to not cause hot or cold spots larger than ±2% of the fraction dose [4], that could be clinically critical. Since a wrong measurement of the beam current and position in the beamline can contribute to errors at the isocenter, as this is related either to a wrong dose given to the tumor volume or an irradiation of a healthy tissue, these parameters must be measured accurately with minimum beam disturbance [5], in addition to the treatment, verifying dose and position measurements just before the patient.

The beam current downstream of the degrader until the coupling point of the gantries is in the range of 0.1–10 nA and is typically measured with thin planar ionization chambers (ICs) as described in [6, 7]. At PSI, these ICs which are permanently inserted in the beamline, provide total current measurements, and are used by the machine control system and by the patient safety system. Since these intercept the beam [8, 9], and can have a negative influence on the physical treatment quality due to compromised beam properties as described above, a dielectric-filled reentrant cavity resonator [10] has been developed as a non-interceptive beam current monitor (BCM) at PSI. The successful measurement of beam currents in the range 0.1–10 nA for energies 238–70 MeV with this cavity beam current monitor (as reported in [11]) provided the motivation to investigate the feasibility of a resonant cavity system for beam position measurements. Such a non-intercepting BPM system in the beamline could be utilized for on-line position control to center the beam that could eventually help simultaneous optimization of the beam everywhere before the gantry coupling point. Simultaneously, online monitoring of beam current and position in the beamline could be used to perform reliable and fast measurements to verify machine settings and to provide feedback to yield improved beam delivery.

The precision demand for the position measurement in the beamline is ±0.5 mm. For PSI, this is a factor three smaller than the precision demand of the beam position at the isocenter, which is ±1.5 mm (corresponds to ±2% of the fraction dose) [4] and is considered sufficient to ensure sufficient homogeneity of the delivered dose distribution. The required precision of the beam position at the isocenter is also facility dependent as it depends partly on the irradiation spot size and the spot spacing used as can be seen in [4].

2022 JINST 17 P09013

Generally, a non-interceptive beam position monitor (BPM) system couples to either the electric or the magnetic field of the beam. These fields are dependent on the transverse beam position in an electrically conducting beam pipe and a high sensitivity measurement of the field distortion can provide accurate information on the beam position.

In PROSCAN the use of broadband non-interceptive monitors for intensities in the range of 0.1–10 nA, is not feasible due to their high level of thermal noise and the associated high detection threshold as discussed in [10]. We found, however, that the resonant measurement of the transverse magnetic dipole mode, TM_{110}, might offer good possibilities for beam position measurements [12] at PROSCAN. The amplitude of this mode is proportional to the off-center position while a resonant system provides a better detection compared to non-resonant systems. In addition, with a single frequency of interest, a narrow bandwidth detection system provides a better signal to noise ratio. The cavity BPM is tuned to the second harmonic of the proton bunch repetition rate since the second harmonic is less prone to interferences from the cyclotron RF system which are mainly concentrated in the first (fundamental) harmonic signal. Moreover, the amplitude of the second harmonic is larger compared to the other higher harmonics because of the bunch length.

These considerations motivated the development of a new type of BPM based on the combination of two pairs of dielectric-filled reentrant cavity resonators to measure the beam position along the X-axis and the Y-axis, respectively, mounted in a common grounded cylinder. In this paper, we explain its working principle, some design considerations, and present the expected performances in term of position sensitivity and required signal integration time. We compare these expectations with test-bench measurements as well as with results obtained during beam operation. For sake of readability, we present our major results in the following sections, the detailed graphs and tables are given in [13]. A more detailed description of the device is given in [14].

2 Dipole mode (TM_{110}) cavity characterisation

In this section, a brief characterization of the dipole TM_{110} mode is presented for a generic pillbox configuration, which is conceptually the simplest type of cavity. An analytical formulation to estimate the pickup signal for a given position offset is given for this starting point of the BPM design. The detailed theoretical backgrounds used in this section can be found in [12, 15–17].

2.1 Modes in a pillbox cavity

For our application, the transverse magnetic modes TM_{mnp} are the most relevant. The notation m, n and p refer to respectively the number of full periods in the azimuthal, radial, and longitudinal direction. The dipole mode TM_{110} is azimuthally asymmetric, and its electromagnetic field distribution is shown in figure 1 (b and c). Its amplitude is proportional to both the beam intensity and to the beam transversal position offset with respect to the center of the cavity. It is important to realize, that there is no difference in amplitude between the opposing sides (e.g., left and right), but that on both sides the amplitude increases with beam offset and intensity. Also playing a role in our application is the monopole mode, TM_{010}, its amplitude is proportional to the beam intensity only. The TM_{010} mode is symmetric in the azimuthal dimension, as shown in figure 1 (a). Though the resonance frequency of the cavity resonator for this monopole mode is lower than that for the dipole mode, it still has an influence on the measurements (see e.g., figure 6).

2022 JINST 17 P09013

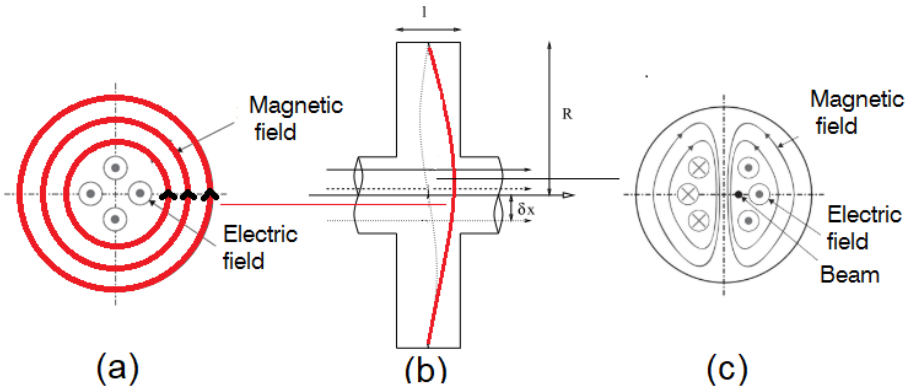

Figure 1. Schematic representation (adapted from [16]) of (a) monopole (TM_{010}) and (c) TM_{110}dipole mode in a generic cylindrical cavity (b).

For a simple pill box the resonance frequency of the TM_{110} mode is given by [17]

$$\omega_{110} = \frac{1}{\sqrt{\mu_o \varepsilon_o}} \frac{a_{11}}{R_{res}} \tag{2.1}$$

where, R_{res} is the cavity radius; a_{11} the first zero of the first-order Bessel function, J_1; $\mu_o = 12.57 \times 10^{-7} H/m$; $\varepsilon_o = 8.854 \times 10^{-12} F/m$.

The fields of the TM_{110} mode, ignoring the effects of coupling ports and beam pipe, are given by [11, 12]:

$$E_{z,110} = C_{110} J_1 \left(\frac{a_{11} \delta x}{R_{res}} \right) \cos\phi \, \exp(i\omega_{110} t) \tag{2.2}$$

$$H_{r,110} = -iC_{110} \frac{\omega_{110} \varepsilon_o {R_{res}}^2}{a_{11}^2 \delta x} J_1 \left(\frac{a_{11} \delta x}{R_{res}} \right) \sin\phi \, \exp(i\omega_{110} t) \tag{2.3}$$

$$H_{\phi,110} = -iC_{110} \frac{\omega_{110} \varepsilon_o R_{res}}{a_{11}} J_1{}' \left(\frac{a_{11} \delta x}{R_{res}} \right) \cos\phi \, \exp(i\omega_{110} t) \tag{2.4}$$

where, C_{110} is proportional to the amplitude of the oscillation and δx is the beam position offset.

2.2 TM_{110} induced voltage

The voltage for a given offset, δx, induced by a charge, q, is derived from the line integral of the eq. (2.2) along the particle trajectory and expressed in terms of the instantaneous voltage at the maximum of the E-field is given by [12]

$$V_{110}^{in}(\delta x) = \omega_{110} \, q \left(\frac{R}{Q_0} \right) \left\langle \frac{a_{11} \, \delta x}{2 J_1^{max} R_{res}} \right\rangle \tag{2.5}$$

The term in the angle bracket is the beam coupling coefficient. The voltage coupled out from the cavity into a $Z_{in} = 50\,\Omega$ measuring system, for a single bunch excitation is expressed in terms of the induced voltage and the loaded quality factor, Q_L, as

$$V_{110}^{out}(\delta x) = V_{110}^{in}(\delta x) \sqrt{\frac{Z_{in}}{\left(\frac{R}{Q_o}\right) Q_L}} \sqrt{1 - \frac{Q_L}{Q_0}} \tag{2.6}$$

2022 JINST 17 P09013

The relationship between the loaded (Q_L) and unloaded (Q_0) quality factor can be found in [10]. The complete set of equations for fields and signals of the TM_{110} mode and their derivation can be found in [12].

3 Design considerations for the TM_{110} cavity

The design choice of the BPM is based on the successful experience with the cavity BCM [10]. The resonance frequency of the TM_{110} mode in the cavity BPM is fixed at 145.7 MHz, the second harmonic of the beam repetition rate, which has the highest signal-to-noise and signal-to-background ratio: it has less RF interference compared to the fundamental and its amplitude is higher than that of still higher harmonics.

Also, the amplitudes of the higher harmonics will be relatively reduced even more for lower beam energies because of the increase of the bunch length due to the increased energy spread at lower energies. This increase of the bunch length downstream of the degrader originates in the degrader which is used to modify the energy during the treatment. The energy degradation results in a beam with an increased momentum width [18] or velocity spread in the velocity. This momentum spread in the beams increases with lower energy. The related spread in velocity causes an increase of the length of the individual bunches in the beam that is proportional to the distance between degrader and BPM. This has also been observed in [19–21]. As a consequence, the instantaneous beam current during the pulse is reduced for the same average beam current [22]. This increase of the pulse length will decrease the amplitude factor (eq. (4.6) in [22]) of the harmonics and thus reduce the response for smaller energies from the cavity BPM.

The BPM design consists of four aluminum LC cavities, suspended within a common grounded cylinder of the same material. These four LC cavities are electrically insulated from each other using a support platform of PEEK, the properties of which are given in [23]. Simulations have shown that an electrically conducting contact between the LC cavities would give a smaller position dependent signal in the TM_{110} mode.

The common dielectric-filling in the reentrant gap of the four LC cavities is a disk of high purity (99.5%) alumina, the properties of which are given in [24]. The high relative permittivity of alumina allows the overall cavity system to be compact while a high TM_{110} mode quality factor, Q_0, can be achieved thanks to its very low loss factor. This results in a larger amplitude of the TM_{110} mode excitation within the cavity for a given beam current and thus in a higher amplitude of the signal coupled out from the cavity.

The TM_{110} mode signals induced by the beam offsets are transferred to the measurement system via a coupling loop in the inductive region of the cavity BPM.

Due to space constraints, a slot, or a waveguide to minimize the signal contributions from other modes has not been considered. The dimensions of the cavity BPM system, matching the TM_{110} mode resonance frequency at 145.7 MHz have been determined from HFSS simulations and are given in figure 2 (detailed dimensions given in figure 4.11 in [14]).

2022 JINST 17 P09013

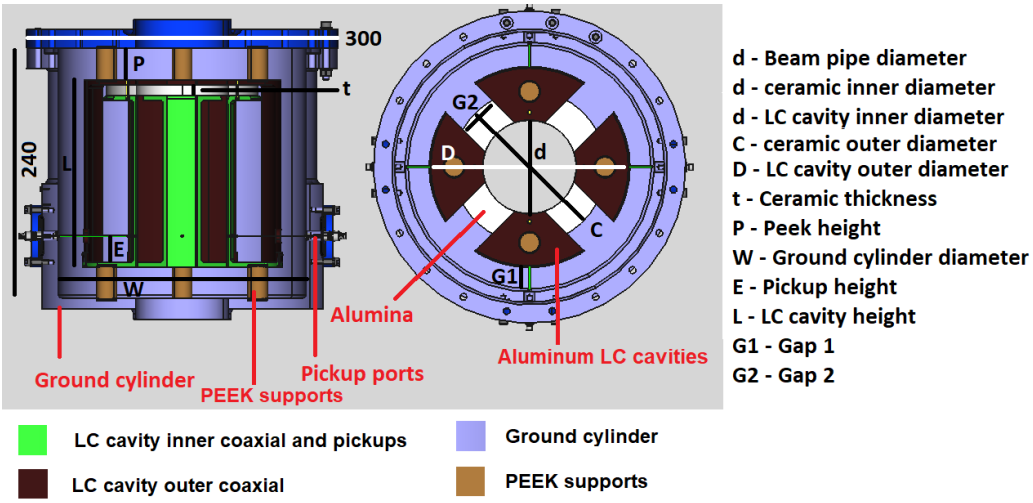

Figure 2. Cut plane of the cavity BPM prototype derived from the HFSS simulation. Dimensions are in mm. The white line representing the parameter D (right image) also represents the cut-plane for the left image. An isometric projection of the BPM can be found in figure 4 (bottom image).

4 Simulation results and design choices

The dimensions of the cavity BPM are derived by using the Eigenmode and Driven modal solvers of ANSYS HFSS [25]. The cavity parameters that are characterized include the unloaded and loaded quality factors, the beam-pickup coupling coefficients, and the inter-pickup (between the floating cavities) coupling coefficients.

4.1 Solutions of the unloaded cavity

The Eigenmode solver takes into consideration the wall conductivity and the dielectric properties of the materials. The solver was configured such that it provides initial dimensions of the cavity BPM without the influence of the measurement ports such that the TM_{110} mode frequencies are as close as possible to the required 145.7 MHz.

The induced fields for the TM_{110} mode of the cavity BPM are shown in figure 3. The field configurations are plotted at the resonance frequencies of the horizontal and vertical polarizations determined by the solver. The calculated unloaded quality factors of the cavity BPM for horizontal and vertical polarizations is $Q_{110} = 3160$. The calculated TM_{110} mode resonance frequency for both the horizontal and vertical polarizations is 145.06 MHz. The values for both polarization directions are equal within the expected accuracy of the calculation. The Eigenmode solutions are exported to the Driven modal solver to fine-tune the cavity BPM with measurement pickups. Minimizing the difference of the TM_{110} mode resonance frequencies of the Eigenmode solution with the design requirement is part of this fine-tuning process.

4.2 Parameters influencing the behaviour of the cavity BPM

The driven modal solver calculates the RF energy propagation within the BPM model and provides the couplings between the different ports of the system S_{ji} (Scattering parameters) [26]. The BPM

2022 JINST 17 P09013

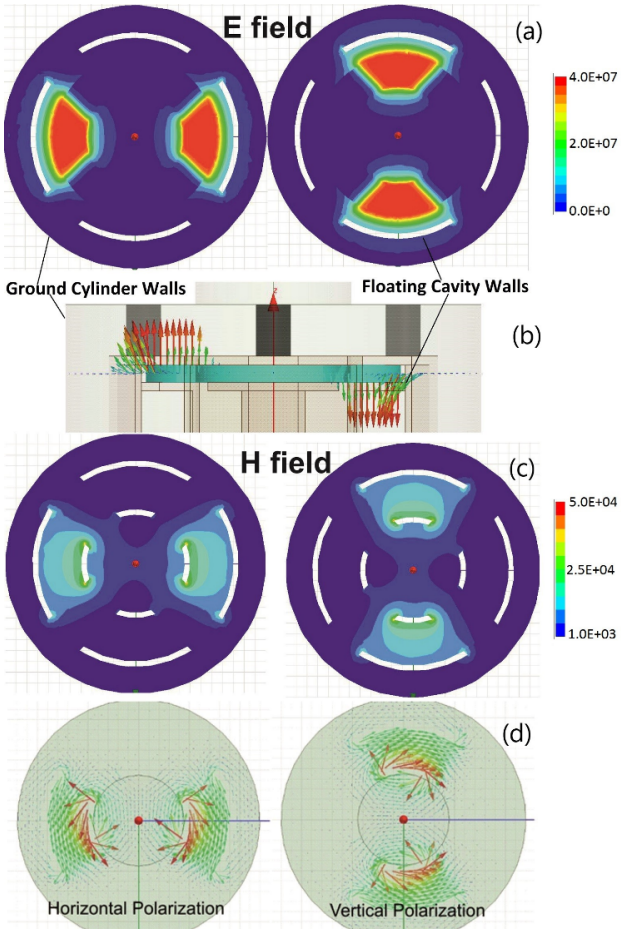

Figure 3. E and H fields (magnitude and vector) of the TM_{110} mode excited within the cavity. The left side represent the horizontal polarization (for offsets in X axis) and the right represent the vertical polarization (for offsets in Y axis). As indicated in b, the E field is plotted on the center plane of the dielectric cross-section. The H field (c and d) is plotted at the plane 30 mm (refer dimension E in figure 2) above the base of the floating cavities. The outer boundary represents the conducting surface of the outer grounded cylinder. The edges where the field terminates represent the conducting surface (boundary termination) of the floating cavities. The Dipole mode is localized within the floating cavities.

model is analyzed using a thin perfectly conducting wire to simulate the stretched wire representing the beam in the test bench setup. Prior to extracting the dimensions of the prototype, certain geometrical parameters of the cavity BPM model are investigated to determine their influence on the operation of the cavity BPM. These parameters are (see figure 2) the inter-cavity gap G2; the intra-cavity (with respect to ground cylinder) gap G1; dielectric width C-d; the dielectric thickness t and the pickup position E. These parameters affect the properties of the cavity BPM (TM mode resonance frequencies, loaded quality factors and position sensitivity). They have been tuned to maximize the position sensitivity. Referring to figure 2, optimal values have been achieved by:

- Increasing the normalized shunt impedance (R/Q_0) by reducing the effective gap radius (either by modifying, G2 or by modifying C-d) and by increasing the dielectric thickness t.

2022 JINST 17 P09013

- Increasing the beam coupling coefficient B_c by reducing the effective gap radius (either by modifying, G2 or by modifying C-d).

- Decreasing the loaded quality factor Q_L by the increasing the loop area, and the inter-cavity gap G2.

The effective gap radius which can be influenced either by the choice of a dielectric (along with its dimension) or by the gap, G2. For instance, the optimization of the gap, G2, is in the azimuthal plane and of the dielectric ring is for a fixed inner diameter. Since either of the optimization does not affect the beampipe radius, these are not an important constrain to where it might fit in a particle therapy beamline for a given operating frequency of the cavity BPM.

All parametric investigations were performed for beam offsets of 0 mm (the center position) and 2 mm. The driven modal simulation setup for the parametric investigation setup is as shown in figure 4.

The $S_{(beam\text{-}pickup)}$ of measurement port 3 (figure 4) for multiple dimensions of the gap G2 is shown in figure 5. The $S_{(beam\text{-}pickup)}$ plots of the other investigated parameters and the investigation results are summarized in [13].

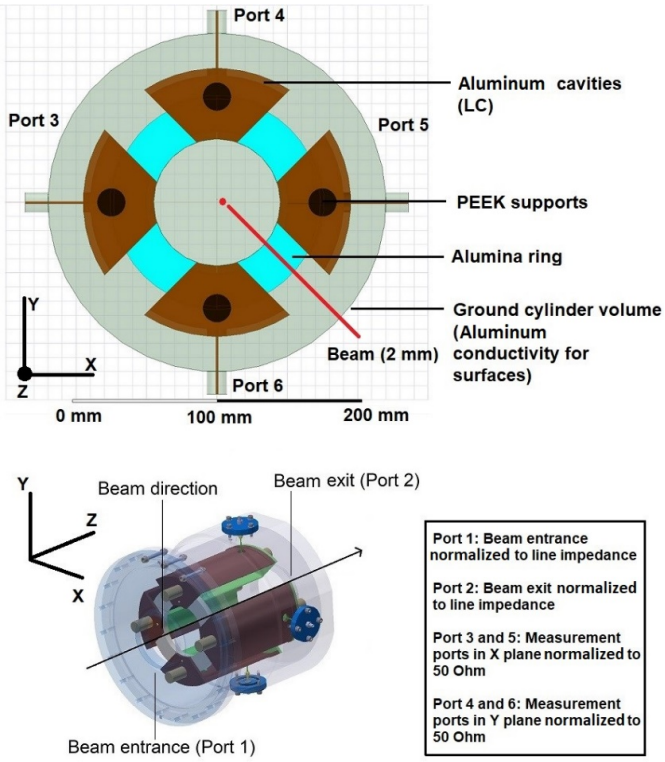

Figure 4. 3-Dimensional view of the BPM and the sketch of the parametric investigation setup. A beam analog is fixed at a position offset of 2 mm towards the LC cavity of interest. The impedance of all the measurement ports is 50 Ω. The impedance of the beam entrance and exit ports corresponds to the characteristic impedance of the coaxial transmission line that the beam analog forms with the cavity inner walls. Scaling for the XY axis in top image.

2022 JINST 17 P09013

The simulation results in figure 5 show that an increase of the gap G2 increases the TM_{010} mode resonance frequency due to a decrease in the gap capacitance. The TM_{110} mode resonance frequency, however, is not increased by the same proportion probably due to the relatively stronger influence of the stray capacitance (i.e. the mutual capacitance between the individual floating cavities and that with the ground cylinder) on the TM_{110} mode lumped element equivalent circuit. Moreover, increasing the gap G2 lowers the loaded quality factor since a larger surface area of the ground cylinder is now available for power dissipation. As a result, we observe an increase in the TM_{010} mode superposition at the TM_{110} mode resonance frequency. The combination of the reduced frequency separation between the TM_{010} and the TM_{110} modes and the reduced loaded quality factors of the modes reduces the effective position sensitivities represented by the difference between the center position (dotted line in figure 5) and the 2 mm position (solid line in figure 5) at the TM_{110} mode frequency (even numbered markers in figure 5).

The gap G1, affects the frequency separation between the modes and their loaded quality factor only weakly in comparison with gap G2 and as a result the position sensitivity is nearly unaffected. However, it influences the coupling strength of the cavities to the beam at the TM_{110} mode resonance frequency (AF 1 in the [13]).

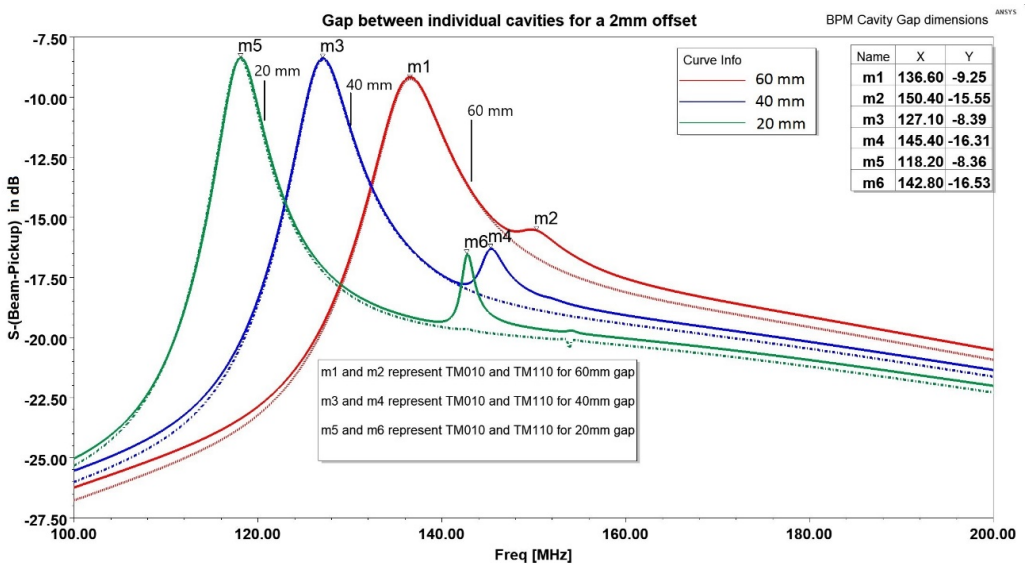

Figure 5. Simulated $S_{(beam\text{-}pickup)}$ of the measurement port 3 (see figure 4) over a frequency span of 100–200 MHz. All the curves are for a position offset of 2 mm for three different inter-cavity gaps (G2): 20 mm, 40 mm, and 60 mm. Odd markers represent the TM_{010} modes and the even markers the TM_{110} modes of the cavity BPM. The dotted lines represent the S-parameter curve for the center position.

The width and thickness of the dielectric help in tuning the resonance frequencies of the modes in the cavity BPM. For a given thickness, increasing the dielectric width (by increasing the outer radius for a fixed inner radius), reduces the TM mode resonance frequencies. And, for a given width, an increase of the thickness, increases the TM mode resonance frequencies by the same extent. However, changing the dielectric width or thickness does not affect the loaded quality factors of either modes and thus, the position sensitivity of the TM_{110} mode remains nearly unaffected by the dielectric dimensions (see AF 2 and AF 3 in [13]).

2022 JINST 17 P09013

The pickup position has minimal influence on the TM mode resonance frequencies since its effect on the inductance of the cavity is small. However, increasing the pickup area reduces the loaded quality factors of the modes which affects the position sensitivity as the contribution of the TM_{010} mode at the resonance frequency of the TM_{110} mode is increased (see AF 4 in [13]). A high loaded quality factor would result in increased sensitivity, but it makes the resonance frequency of the TM_{110} mode sensitive to e.g. temperature variations and external vibrations and it requires a higher mechanical accuracy in the assembly.

From these investigations, the dimensions (see figure 2) of Gap G1 as 25 mm, Gap G2 as 40 mm, pickup position E as 30 mm, dielectric width C-d as 28.57 mm and dielectric thickness t as 10 mm for the prototype BPM were chosen to obtain a reasonable frequency separation between the resonance frequencies of the modes, optimum loaded quality factor of the TM_{110} mode and thereby good position sensitivity. The results of the parametric investigation are summarized in AT 1 in [13].

4.3 Cavity BPM prototype simulations

In this subsection, BPM simulation results are presented for different beam positions. The consequences of the superposition of the TM modes at the measurement frequency, the effect of cavity-position errors and the influence of dielectric-loss factor on the performance of the BPM are investigated.

Beam position related signal. The analysis of the cavity BPM response to the beam position is performed at different position offsets of the beam (0 mm, 2 mm, 5 mm, 10 mm and 15 mm) towards a given single cavity on the X axis. Due to the symmetry of the dipole mode field and the cavity BPM and the $S_{(\text{beam-pickup})}$ behavior of the other cavities is assumed to be the same and the results are summarized for a single cavity with measurement port 3 in table 2.

In figure 6, the $S_{(\text{beam-pickup})}$ behavior of both the X plane cavities and the Y plane cavities are plotted for a position offset of 2 mm towards measurement port 3 (see figure 4). The markers for the curves S-41 and S-61 (port 4 and 6) represents the coupling coefficient for the zero coordinate of the Y axis which is the center position information. This is representative of the tail of the position independent monopole mode. The TM_{010} mode resonance of the cavity BPM is at 127.1 MHz and the TM_{110} mode resonance at 145.7 MHz. The simulation results for different position offsets are evaluated from the S-transfer matrix (AT 2 in [13]) of the cavity BPM according to eq. (9) taken from [27]

$$Z_{tr,i} = \frac{S_{1i}}{S_{12}} \sqrt{Z_o Z_c} \tag{4.1}$$

where S_{12} is the transmission coefficient between beam entrance and beam exit port; S_{1i} is the transmission coefficient between the beam entrance and the measurement ports (3,4,5 or 6) for a given offset; Z_o is the impedance of the measurement port, $Z_o = 50\,\Omega$ and Z_c is the characteristic impedance of the coaxial transmission line that the beam analog forms with the cavity inner walls, $Z_c = 366\,\Omega$.

The cavity BPM's sensitivity which is given by the slope of the linear relationship between the pickup voltage and the position (given in table 2) from the simulation and is approximately 2.25 nV/nA·mm. For a 0.1 nA beam current, for every subsequent 0.5 mm increase, the signal power will increase by approximately 0.6 dB.

2022 JINST 17 P09013

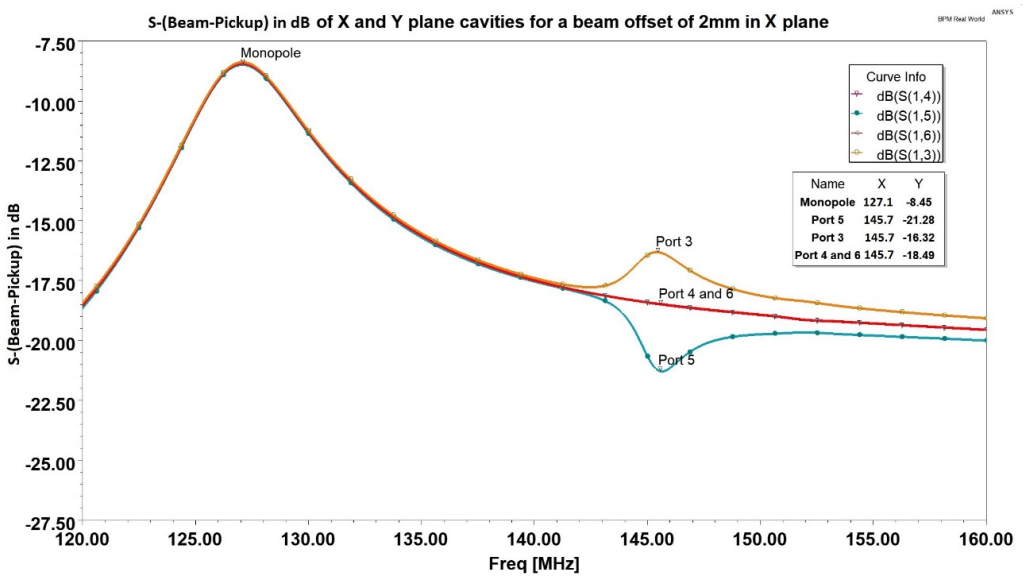

Figure 6. $S_{(beam\text{-}pickup)}$ transmissions for X cavities (ports 3 and 5) and Y cavities (ports 4 and 6) for a beam offset of 2 mm in X plane. Port 3 and Port 5 markers represent beam-pickup coupling coefficient of the X plane cavities whose TM_{110} mode excitation is represented as maximum and minimum of the S-plots. The Monopole marker represent the TM_{010} mode resonance frequency and its amplitude. Port 4 and 6 markers represent the TM_{010} mode amplitude at the TM_{110} mode resonance frequency, which is the zero-position information.

Table 2. $S_{(beam\text{-}pickup)}$ for port 3 measured over a 50 Ω impedance for a beam intensity of 1 nA.

X Position (mm)	S31 (dB)	Pickup Voltage (nV)
0	−18.45	16.2
2	−16.32	20.5
5	−13.78	27.5
10	−10.81	38.7
15	−8.63	49.7

Mode superposition. Simulation of the cavity BPM without the beam analog shows that there are three modes present within the frequency range of 120–160 MHz. These modes are identified as TM modes from the HFSS solver as TM_{010} at 127.5 MHz, TM_{110} at 145.7 MHz and TM_{210} at 152.5 MHz and is shown in the S-transmission (between ports 3 and 5) of the cavity BPM's in-plane cavities (figure 7).

We require a strong coupling between the beam and the pickups at the TM_{110} mode resonance frequency to obtain accurate position information of the low-current proton beams (0.1–10 nA). But a demand for a stronger pickup coupling reduces the loaded quality factor of all the TM modes, which contributes to unavoidable superposition of the modes at the frequency where the measurement is performed. For the position measurement, only the superposition between the stronger TM_{010} mode and the weaker TM_{110} mode is of concern. The presence of TM_{210} mode at 152.5 MHz does not contribute significantly to the superposition as it a weaker mode compared to TM_{110} mode.

2022 JINST 17 P09013

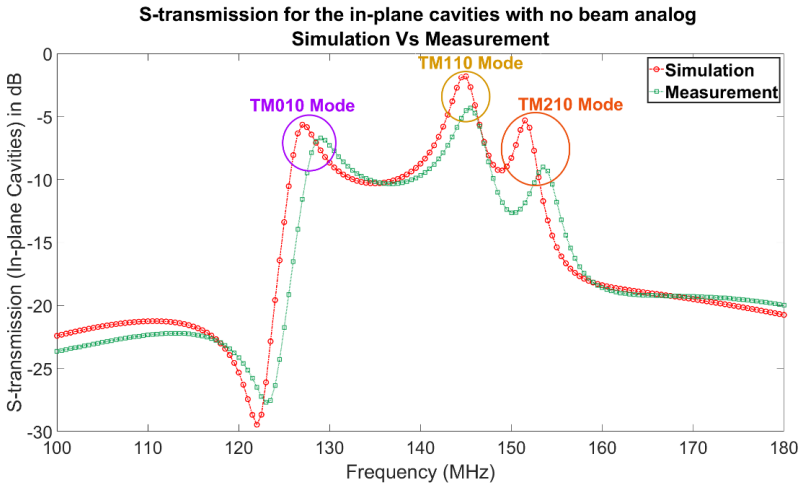

Figure 7. Measured S-transmission for in-plane cavities (X-axis) (with no beam analog) compared with simulation. Marked in circles are the modes that can be excited in the structure between 120–160 MHz.

The presence of multiple TM modes within a narrow frequency band is mainly due to the required compactness of the cavity BPM. However, the superposition between the TM_{010} and the TM_{110} mode can also be considered a benefit, as it allows to determine the sign of the position offset signal without the need of another cavity device as a reference as recommended in [16]. This is clearly demonstrated in figure 6 by the maximum amplitude for port 3 and the minimum amplitude for port 5. Moreover, for increasing beam displacement towards a cavity along a given axis (here the X-axis), the $S_{(\text{beam-pickup})}$ coefficient (maximum) at the TM_{110} mode resonance frequency increases with no shift in frequency. This is due to the small relative phase difference between the TM_{010} and the TM_{110} modes with respect to the drive signal at the resonance frequency of the TM_{110} mode. However, for the other cavity along the same axis, with increasing beam displacement away from the center, the minimum of the $S_{(\text{beam-pickup})}$ shifts in frequency since the relative phase difference between the TM_{010} mode and the TM_{110} mode at the resonance frequency of the TM_{110} mode is higher and has a stronger frequency dependence (see figure 8).

As can be seen in the pill-box configuration in figure 1 (a and c) and the H-field polarization directions in figure 3 (d), the vector addition of the amplitudes of the TM_{110} and TM_{010} modes gives a different result for the left and the right cavities. This is due to opposite curl orientations of the induced magnetic fields between the TM_{010} and TM_{110} modes in the cavity for beam displacements away from the center. This is a unique feature of the cavity BPM, where the effect of this mode superposition can be used as an advantage to have complete position information (magnitude and sign), so that there is no need of an external sign detection, by means of a reference cavity sensitive to only the TM_{010} mode. Another important feature of the cavity BPM is that the TM_{110} mode's vertical polarization is not excited for pure horizontal offsets and vice versa. This enables to measure X and Y beam position offsets independently as there is no interference between the signals caused by them.

Cavity asymmetries and dielectric-loss factor. The agreement between calculated and measured performance of the cavity BPM is dependent on the symmetry of the actual cavity system and the electrical properties of the alumina ring. Unfortunately, asymmetries such as small errors in the

2022 JINST 17 P09013

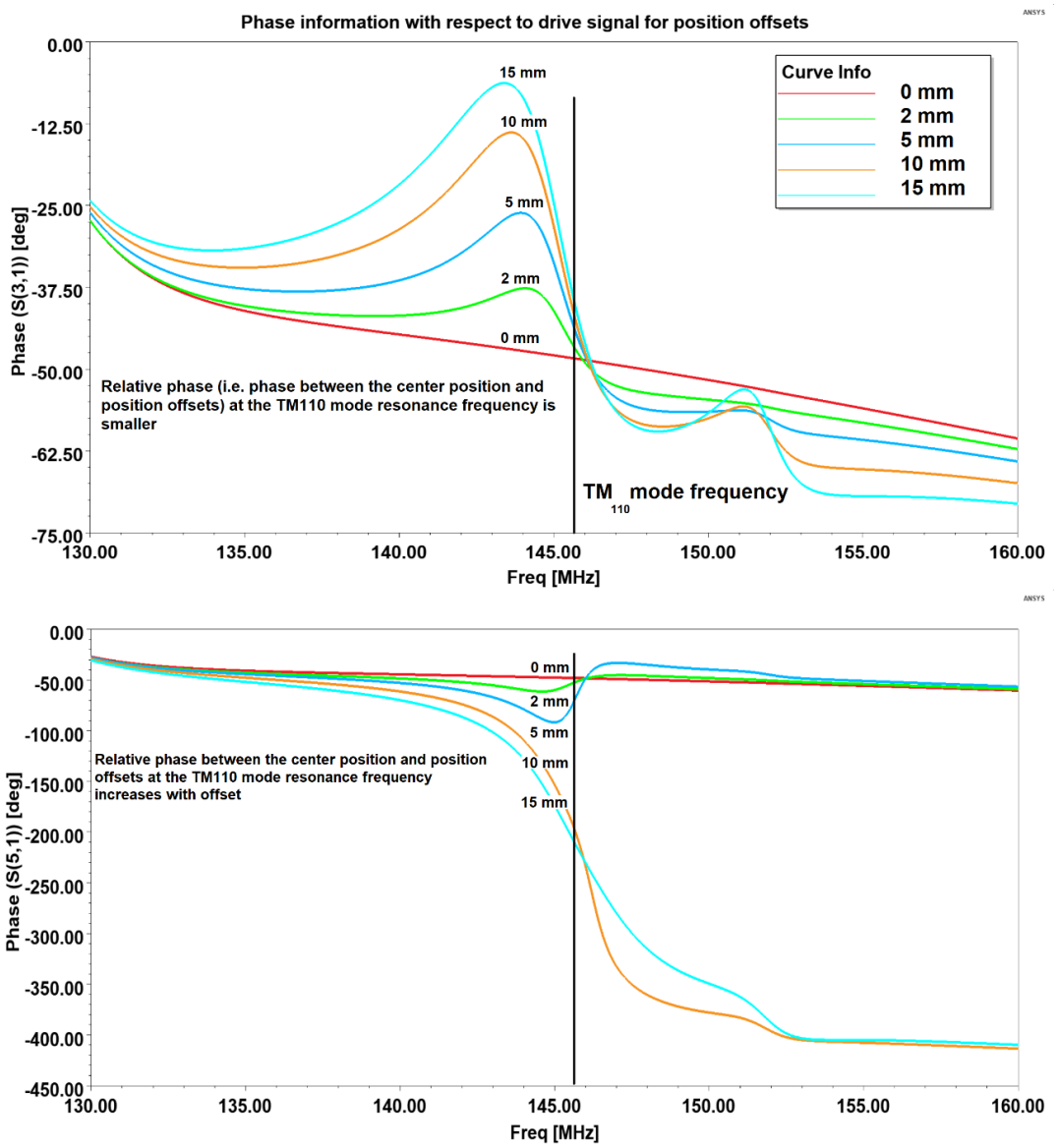

Figure 8. Phase information of the pickups corresponding to ports 3 and 5 (figure 4) with respect to the beam entrance port for different position offsets. At the TM_{110} mode resonance frequency i.e. 145.7 MHz, the increase in the relative phase between the center position and the position offsets with increasing offset is smaller for the pickup corresponding to port 3 and is larger for the pickup corresponding to port 5.

position and axial orientation of the cavities, and position errors of the dielectric ring cannot be completely avoided in the actual realization. These asymmetries can be estimated with a 3D coordinate-measuring machine (CMM) and for a mechanically robust design, a reliable device can be built that needs calibration only once.

In the simulations, we studied how the asymmetries of a cavity in a given plane affect its position sensitivity in that plane and the TM_{110} mode resonance frequency for a beam offset of +2 mm. For instance, a cavity position error of 0.50 mm from its symmetric position towards the center causes its TM_{110} mode resonance frequency to decrease by approximately 300 kHz. For a real beam current

2022 JINST 17 P09013

of 1 nA and with a bunch length of 2 ns, the signal that corresponds to the 2 mm position offset is then 5.8 nV above that for a centered beam instead of 4.3 nV (see table 2). Similarly, for the same position error but in the opposite direction, the cavity's TM_{110} mode resonance frequency is increased by 300 kHz and its signal level for a 2 mm position offset is only 3.3 nV higher than that for the centered beam. So a position error of one of the cavities by 1 mm could result in a measurement error of 1.1 mm. Similarly, a rotation error of a cavity around the Z axis by 17.45 mrad (1 degree), leads to a measurement error in that plane of approximately 0.15 mm and a measurement error in the orthogonal plane by approximately 0.40 mm due to an increased XY crosstalk. The TM_{110} mode resonance frequency is changed by 100 kHz only in this case.

A position error of the dielectric (alumina) ring does not affect the TM_{110} mode resonance frequency of the cavities but affects the position sensitivity. For a dielectric position error of 0.5 mm from its symmetric position towards a cavity in a given plane, the cavity's signal for a 2 mm position offset is only 1.8 nV higher than that for a centered beam. The same cavity's signal for the same offset is 7 nV higher than that for a centered beam when the dielectric is displaced by the same amount in the opposite direction. This corresponds to a measurement error of approximately 2.4 mm. In addition to these asymmetries, the cavity BPM's position sensitivity at the TM_{110} mode frequency is strongly dependent on the dielectric constant (ε_r) and the dielectric loss factor (δ). The dielectric constant, ε_r, of the alumina ring should be within 1–2% of $\varepsilon_r = 9.8$ and a loss-factor, δ, of 2.0×10^{-4} to have measurement results in perfect agreement with the simulation. For a loss-factor of 3.0×10^{-4}, the position sensitivity is reduced by approximately 7%.

To have minimal position error from all possible asymmetries, a strict demand needs to be place on a robust design, verification of the assembly process using 3D CMM and a strict tolerance for the installation in the beamline in addition to the demand to use a high purity alumina. An overall tolerance in linear position errors of at most 0.05 mm and in rotational errors of at most 2 mrad is advised to have similar results to simulation.

5 Test-bench measurements

The cavity BPM prototype has been characterized in a test bench by moving a thin stretched wire with two motorized precision stages in the X or Y direction [28]. The test-bench results and the simulation estimate are shown in figure 9 (also in figure 7 without the beam analog). The results in figure 9 are measured at the TM_{110} mode resonance frequency of the individual cavities. The cavities in the X-plane have their TM_{110} mode resonance frequency at 146.0 MHz and the cavities in the Y-plane at 148.1 MHz. The TM_{110} mode resonance frequency is different from 145.7 MHz because of a mechanical reassembly. The mechanical reassembly procedure involved disassembling the LC cavities and the PEEK supports and reassembling them together following a 3D CMM to confirm the asymmetry. The reassembly's objective was to improve the pickup coupling coefficient and was useful as it helped to improve the position sensitivity of the BPM which was approximately 75% lower than the simulated position sensitivity before the reassembly. After correcting (qualitative) for any potential asymmetries with a reassembly, the signal sensitivities of the pickups were measured to be within 5% of the simulated estimate for the center position and to within 16% for a 15 mm position offset. The position sensitivity of the pickups also was improved to within 23% of the simulation estimate following the reassembly. Since the reassembly was based on simulation

2022 JINST 17 P09013

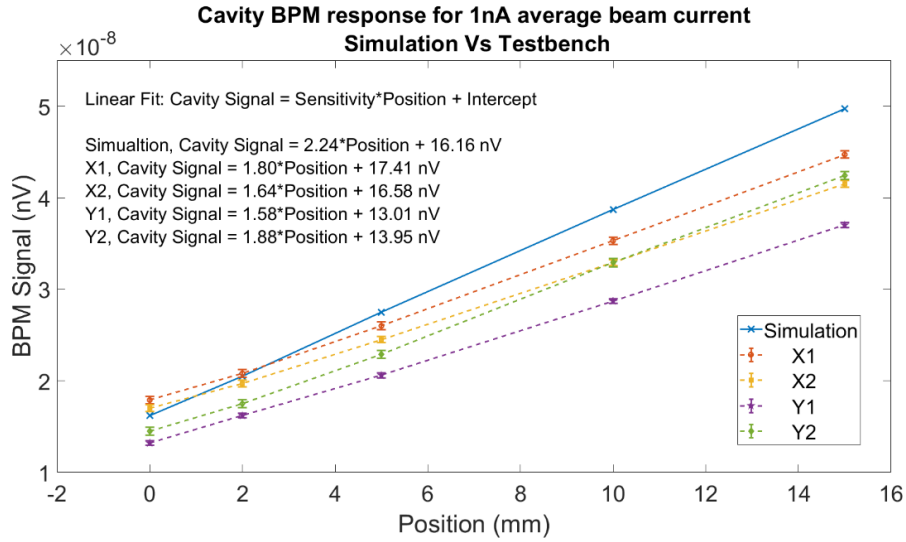

Figure 9. The pickup signal at the BPM for the four cavities is shown as a function of beam position offset (stretched wire moving towards cavity). A comparison of simulation and test-bench measurements is presented.

confirmation of mechanical errors, it is expected that this iterative process was a necessary step in our design process. The remaining difference in the position sensitivity is due to the difference in the dielectric loss factor (a factor 30 higher) of the alumina ring with respect to the simulation value and has been confirmed with simulations. However, due to the reassembly, the shift in the TM_{110} mode resonance frequency of the individual cavities could not be avoided. A detailed description of the effect of reassembly can be found in [14], chapter 4 and 5.

6 Beamline measurements

The BPM prototype in the PROSCAN beamline, which is a temperature-controlled environment (28.5 ± 0.5°C), is located six meters behind the degrader exit; its measurement chain is shown in figure 10. The temperature-controlled environment is essential for reproducible magnetic fields in the beam line, but it is not a necessity for the cavity BPM prototype due to its lower loaded quality factor. For example, for a temperature difference of ±5°C, the change in the length of the cavity is approximately 30 µm. Such a small change in the length does not contribute to major change in the resonance frequencies (~100 kHz) as well as the coupling coefficient (~0.1%). The measurement references for the beam current and position are from a multi wire ionization chamber (IC) located within a meter downstream of the BPM. The IC has a beam current uncertainty of 1% and a beam position systematic uncertainty of maximum ±0.3 mm, respectively. The BPM cavities along the vertical axis, Y1 and Y2, were terminated with 50 Ω and are not used for the measurements since their TM_{110} mode resonance frequency was at 148.8 MHz following a second reassembly before beamline installation. The TM_{110} mode resonance frequencies of the cavities in the X axis was at 146.1 MHz after the second reassembly, sufficiently close to the second harmonic of the repetition frequency to be able to perform the measurements. The raw signals from the BPM cavities in the X-axis were amplified with a low-noise amplifier (R&K- LA130- OS, noise figure 1.7 dB) with a

2022 JINST 17 P09013

gain of 36 dB each and were coupled via 30-meter-long coaxial cables (1/2″ H&S SUCOFEED) to a single channel spectrum analyser outside the beam-line vault [29]. The 30-meter-long cable is expected to attenuate the signal strength by approximately 1–2 dB. The position response of the BPM prototype was verified in relation to its beam current response for different beam energies. In the following subsections these measurements will be described first, followed by a description of a measurement of the response to the beam position.

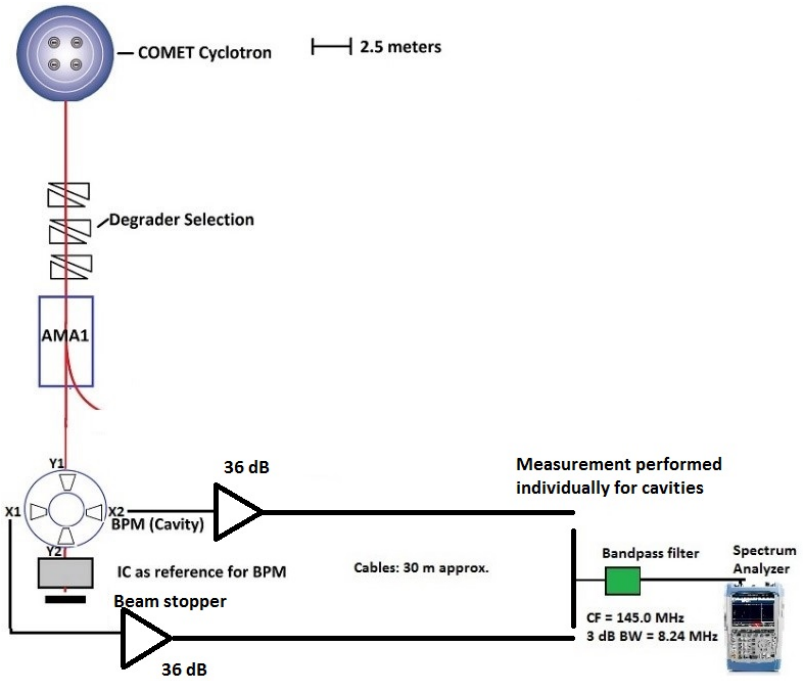

Figure 10. BPM located at six meters from the degrader exit. The measurement chain consists of two 50 Ω impedance low noise-amplifier with 36 dB gain each (located next to the BPM), followed by a bandpass filter (after 30 meters long cables), whose center frequency is 145.0 MHz and its 3 dB bandwidth is 8.24 MHz. A spectrum analyzer, FSH 8 from Rhode and Schwarz, provides amplitude measurement of the BPM for beam position offsets. The measurement is performed separately for each cavity.

For a 200 MeV beam, the beam current sensitivity of the position signal was measured at two different beam offset positions: 2.4 mm and 4.8 mm. The energy dependence has been determined for measurements with a 200 MeV and a 138 MeV beam. We performed a beam current sweep for a given fixed position offset of 4.8±0.3 mm. For a 138 MeV beam, the beam position sweep is performed for two beam current scenarios: 2.6 nA and 12.2 nA. Also, the horizontal cavity response for a vertical beam position sweep is measured to check the non-excitation of the horizontal polarization of the dipole mode for a beam position offset in the vertical direction.

6.1 Beam intensity and energy response

The beam intensity and beam energy dependence are studied with the X1 cavity. The measurement offset of the X1 cavity is the no-beam response when the cyclotron RF is on. This measurement offset is a combination of interference from the cyclotron RF accelerating cavities, background noise, voltage fluctuations from a ground loop at the input of amplifiers, and other possible spurious

2022 JINST 17 P09013

interferences from radio communications [30]. The amplitude of the X1 cavity's measurement-offset is measured as 4.62 µV and is assumed as a constant in the further data analysis.

The beam intensity dependence was measured for the beam current range 0.1–15 nA with a 200 MeV proton beam. The X1 cavity's response after measurement-offset correction is shown in figure 11 (a). For a given position offset, the X1 cavity's beam intensity response is linear and, as expected has higher beam current sensitivity for larger position offsets. The ratio of the beam current sensitivity between 4.8 mm and 2.4 mm offset from the measurement is approximately 9% higher than the ratio from the simulation estimate.

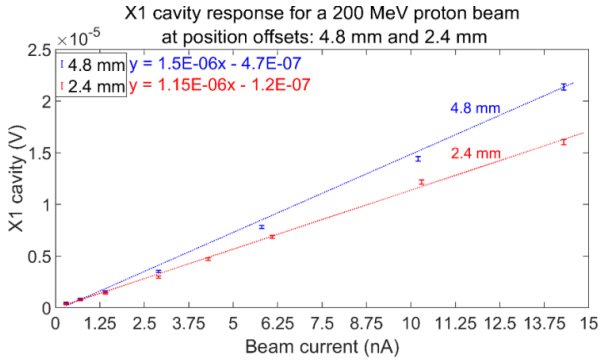

(a)

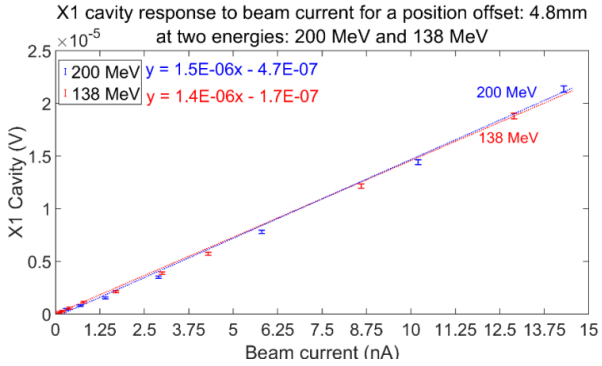

(b)

Figure 11. Shown in (a) is the X1 cavity response with measurement-offset correction for a 200 MeV proton beam at beam positions: 4.8 mm and 2.4 mm towards X1. Shown in (b) is the X1 cavity response with measurement-offset correction for a 200 MeV and 138 MeV proton beam at 4.8 mm towards X1. The error bars of individual data points shown in both the plots constitute two σ measurement uncertainty and were evaluated through error propagation.

A similar measurement is done to study the energy dependence at 4.8 mm for two beam energies of 200 MeV and 138 MeV respectively. At six meters from the degrader exit, the BPM is expected to deliver nearly the same position sensitivity shortly downstream of the degrader due to the small difference (4%) of the bunch lengths between the two energies compared to locations further downstream. The BPM response (of the X1 cavity after offset-correction) as a function of beam current for the two different energies is shown in figure 11 (b). The beam current sensitivity of the X1 cavity, given by the slope of the linear curve, is lower by approximately 3% at 138 MeV compared to 200 MeV, which is in good agreement with the difference in bunch length.

2022 JINST 17 P09013

The X1 cavity's beam current normalized response (AF 5 in the [13]) is a minimum in the range 0.5–2.5 nA. At this moment, we have no clear explanation for this effect. For beam currents higher than 2.5 nA, the X1 cavity response is not influenced by such variations in the measurement offset. A possible explanation for this observation could be the RF interferences which have also been observed in other beam diagnostics in our facility. Their effect is relatively stronger for beam currents lower than 2.5 nA. Thus, for reliable beam position measurements with the spectrum analyzer, beam currents higher than 2.5 nA are used. Note that the measurement offset correction can be improved by applying an I/Q demodulation [31] using a reference signal derived from the cyclotron RF-cavities instead of using a spectrum analyzer. This will not only consider the magnitude but also the phase difference of the no-beam signal with respect to the BPM signal to be measured.

6.2 Beam position response

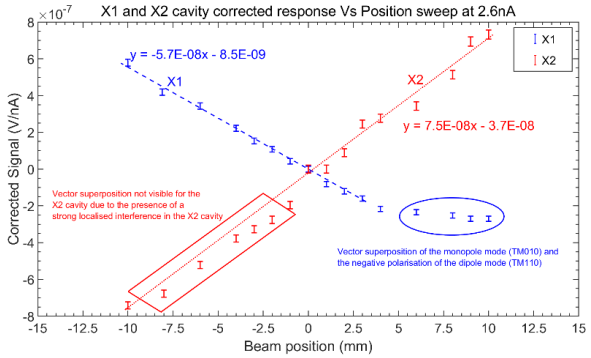

(a)

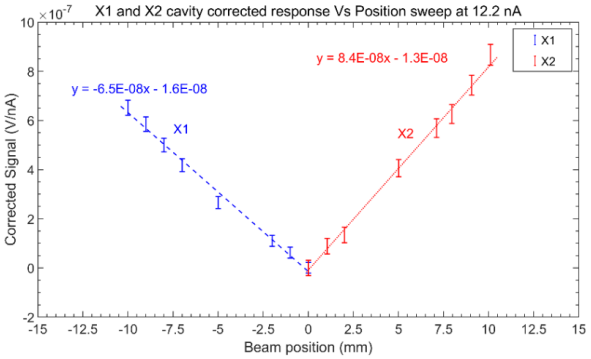

(b)

Figure 12. X1 and X2 cavity signal after measurement-offset correction and beam current normalization plotted vs beam position (X-axis sweep) for beam currents 2.6 nA (a) and 12.2 nA (b). The 2.6 nA measurement scenario shows the vector superposition effect between the stronger monopole mode and the negative polarity of the weaker dipole mode as expected (X1 cavity). For the X2 cavity, this effect is not observed and the origin of this behaviour is not clear. Hence, for the 12.2 nA measurement, the beam is swept in the range 0.0 to +10.0 mm for the X2 and to −10.0 mm for the X1 cavity and only its results are summarised in this subsection. The data points are plotted with a 95% confidence interval ($\pm 2\,\sigma$ uncertainty). Reference beam current and position were measured with a profile monitor (IC type).

2022 JINST 17 P09013

The beam position measurement was performed for a 138 MeV beam with an intensity of 12.2 nA. The beam was swept from −10 mm to +10 mm in the X-direction and signal from the most nearby cavity (X1 or X2) was measured. For the range 0.0 to −10.0 mm the X1 cavity was used and for 0.0 to +10.0 mm, X2 cavity was used, in both cases for a fixed Y-coordinate of the beam close to the center position (Y = 1.05 mm). These offset positions correspond to displacements of the beam towards the corresponding cavities. The FWHM of the proton beam is 20 mm in both the X and Y planes. The X1 and the X2 cavity response after measurement offset correction and beam current normalization are shown in figure 12.

The position sensitivity, given by the slope term in figure 12, is approximately 30% higher for the X2 cavity compared to the X1 cavity. This could be due to the asymmetries induced in the BPM cavities when a reassembly was performed before beamline installation. The effect of asymmetries was confirmed by the shift in the TM_{110} mode resonance frequency of the cavities within the BPM. For the X axis cavities, the TM_{110} mode resonance frequency was shifted to 146.1 MHz while for the Y axis cavities it shifted to 148.8 MHz.

The measurement offset and beam intensity corrected response of the X2 cavity for Y-axis sweeps in the range −10.0 mm to +10.0 mm show that the excitation of the horizontal polarization of the TM_{110} mode for vertical beam positions is much weaker and within its 95% confidence interval can be approximated as a non-excitation. This is shown in figure 13.

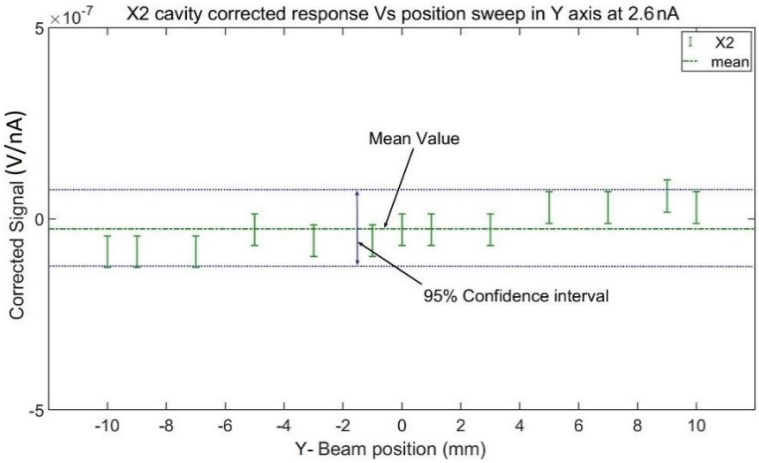

Figure 13. X2 cavity corrected response Vs position sweep in Y-axis over a range −10.0 mm to +10.0 mm. The green line represents the average of the measurement and the blue lines represents the two-sigma uncertainty evaluated from the data set.

The position related parameters of the X1 and X2 cavities are summarized in table 3, which includes sensitivity, systematic uncertainty, and statistical uncertainty. The position sensitivity of the individual cavities is given by the slope term in the linear-fit equations in figure 12. An estimate of the systematic position uncertainty is given by the average of the absolute difference between the reference position and the measured position. This systematic uncertainty includes the effects of the alignment offset and the measurement offset. The reference position has its own systematic uncertainty (±0.3 mm). The statistical uncertainty is given by the standard error for the position estimate.

2022 JINST 17 P09013

Table 3. Measurement summary of X1 and X2 cavities for a 138 MeV beam and a beam current of 12.2 nA.

Position Parameters	X1	X2
Sensitivity, nV/nA mm	64.8±1.7	83.7±2.1
Systematic uncertainty, mm	0.26	0.18
Statistical uncertainty, mm	0.37	0.26

The signal-to-noise ratio (SNR) of the measurement will increase with increasing beam currents. Consequently, it shows clearly that higher beam currents will improve position precision and accuracy.

6.3 Summary of beam measurements

With the beam current sweep and the beam position sweep measurements, we have demonstrated the capability of a prototype dielectric-filled cavity BPM system to measure beam positions in a non-interceptive manner without disregarding the existence of a significant measurement-offset. The measurement summary is as follows:

- Beam position increment of 0.5 mm can be measured for beam currents as low as 0.1 nA *in the case of minimized RF interference* (extrapolating from the measurement summary).
- The systematic position uncertainty of the X2 cavity is 0.18 mm and of the X1 cavity is 0.26 mm.
- The statistical uncertainty of both the X plane cavities is within the 0.5 mm requirement.
- Good agreement between the measured (3%) and expected difference (4%) in sensitivity caused by the beam energy dependence of the bunch length.
- Though not shown here, the quadrant of the beam position offset is identified without the need for an additional cavity in which the TM010 mode is detected (as in conventional cavity BPMs) in [14] by taking advantage of mode interference.

The performance of the cavity BPM in terms of position sensitivity and precision are within the PROSCAN requirements. The position precision could be enhanced further by measuring the measurement offset vector referenced with respect to the cyclotron RF (using RF phase measurement) and applying a model that provides information on the relative phase between the TM_{010} and the TM_{110} modes. From the design perspective, the BPM's performance could be enhanced by minimizing mode superposition and maximizing output signal for a given position offset with further design optimization.

7 Possibilities for improvement

An improvement in the normalized shunt impedance $(R/Q_0)_{110}$, and improved loaded quality factors of the TM_{010} and of the TM_{110} modes is expected through an important modification, which is an increase of the gap thickness with respect to the gap radius. This is achieved by increasing the

2022 JINST 17 P09013

reentrant gap thickness and by reducing the dielectric width. Minimizing the loop area and reducing the gap between the cavities with respect to each other (Gap G2) and with the ground cylinder (Gap G1) also helps in improving the normalized shunt impedance and the loaded quality factors of the TM modes. This should provide an increased output signal for a given position offset. A mechanical improvement of the symmetric mounting of the cavities is planned by replacing the PEEK support rings with support plates along with optimization of other mechanical design parameters to improve the robustness of the BPM. These changes will improve the separation between the TM_{010} and the TM_{110} mode resonance frequencies. Therefore, we expect to reduce the TM_{010} mode superposition at the TM_{110} mode resonance frequency.

With these improvements as described in [14], the signal level for a centered beam is expected to be reduced by 25%, while the position sensitivity would improve by approximately a factor 2.4. The new BPM model has been built and installed in the beamline and measurements with beam have shown an increase in the position sensitivity as shown in figure 14 and are in good agreement with the expectation in sensitivity improvement. The position related parameters of the X1 and X2 cavities in the improvised BPM are summarized in table 4. These cavities have their TM_{110} mode resonance frequencies at 145.7 MHz

Table 4. Measurement summary of X1 and X2 cavities for a 250 MeV beam and a beam current of 9.3 nA.

Position Parameters	X1	X2
Sensitivity, nV/nA mm	167±1.9	216±1.1
Systematic uncertainty, mm	0.06	0.03
Statistical uncertainty, mm	0.1	0.04

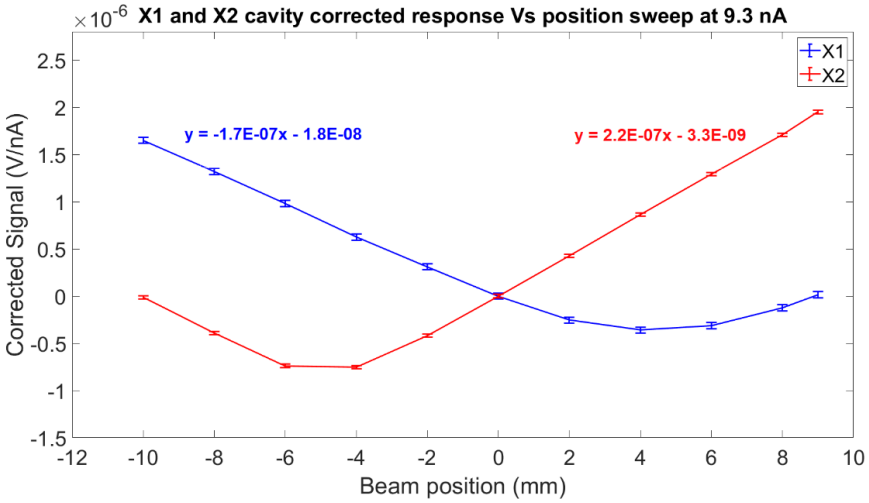

Figure 14. X1 and X2 cavity signal of the improvised BPM after measurement-offset correction and beam current normalization plotted vs beam position (X-axis sweep) for 9.3 nA beam current at 250 MeV. The position is swept from −10.0 mm to +9.0 mm. The data points are plotted with a 95% confidence interval ($\pm 2\,\sigma$ uncertainty). Reference beam current and position were measured with a profile monitor (IC type).

2022 JINST 17 P09013

8 Conclusions

To measure the position offset with respect to the beam axis of a 0.1–10 nA proton beam in the energy range 70–238 MeV, a compact fourfold dielectric-filled reentrant cavity BPM has been built. This cavity BPM is a combination of four floating cavities with a dielectric filling in their reentrant gap. We presented the design of the first prototype system, identified potential improvements in design following measurements and results of experiments with the improvised BPM system. The overall demonstration shows good agreement with the simulation-based expectations.

In the cavities, the resonance frequency of the TM_{110} (dipole) mode is tuned to the second harmonic of the pulse rate of the proton beam (145.7 MHz), which is the frequency at which the signal is measured. At this frequency there still is a strong signal of the TM_{010} mode. In our design, this signal is used as an advantage to identify the sign of the beam offset, so that we can refrain from an external reference cavity to determine the sign of the beam displacement.

The test-bench measurements on the cavity BPM prototype after a mechanical reassembly showed a good agreement of the position sensitivity with the simulation results with a compromise on the TM_{110} mode frequency shifts. The observed differences in frequency and in sensitivity are attributed to asymmetries aroused from the reassembly and to differences in the material properties.

The prototype cavity BPM as well as an improved version of the cavity BPM have been tested in the beamline to validate the dependence of the beam position signal on beam intensity and beam energy. The cavities displayed linear relationship with the beam position offset. For a more accurate measurement of the position sensitivity of the cavities, a vector measurement of the measurement offset i.e. I/Q demodulation with respect to cyclotron RF is expected to be helpful. With a spectrum analyzer and without disregarding the existence of a significant measurement-offset, we have demonstrated that we can achieve a position precision (1σ) better than 0.5 mm.

For a given beam position offset, the dependence on beam intensity was shown to be linear and the dependence of beam energy is as small as expected, due to the BPM's proximity to the degrader exit.

Based on measurements down to 2.5 nA and simulations for lower intensities, we conclude that this cavity BPM is a promising candidate for measuring beam positions of proton beams of low intensities (0.1–10 nA) in a purely non-destructive manner. To our knowledge, this is the first non-interceptive beam position monitor to have demonstrated position measurements in a cyclotron-based proton therapy facility. This cavity BPM could be used for online position control i.e. beam centering to optimize for beam transmission until the coupling point of the gantry and as a redundant system for position verification.

Such a cavity BPM could be of an advantage compared to the typically used ionization chambers (ICs) for the purpose of daily quality checks in irradiations using higher beam intensities, such as in so called FLASH irradiations [32]. Here, beam intensities correspond to pulse charge in the range 10–100 pC delivered within 10 µs and with a pulse frequency of typically 1 kHz, thus making the ICs response non-linear [33]. Moreover, their response saturates for smaller beam size. On the contrary, the cavity BPM is expected to provide a linear and a beam size independent response as can be seen in eqs. (2.5) and (2.6), which show that V_{out} is not dependent on a beam size parameter. For instance, for a 100 nA real beam current and with a measurement resolution bandwidth of 100 kHz, we can make fast measurements (within a signal integration time of tens of microseconds)

2022 JINST 17 P09013

using the cavity BPM as the signal level is expected to be approximately 20 dB above the noise level. The limitation here in terms of measurement speed is not the monitor but would be from the processing electronics.

Acknowledgments

This project received funding from the European Union's Horizon 2020 research and innovation programme under the Marie Sklodowska-Curie grant agreement No. 675265.

Conflicts of interest. The authors declare no conflicts of interest.

References

[1] J.M. Schippers et al., *The SC cyclotron and beam lines of PSI's new protontherapy facility PROSCAN*, *Nucl. Instrum. Meth. B* **261** (2007) 773.

[2] P. Forck, *Lecture Notes on Beam Instrumentation and Diagnostics*, in *Joint University Accelerator School*, Erice, Italy (2011).

[3] G. Kube, *Specific diagnostics needs for different machines*, in *CERN Accelerator School, beam diagnostics*, Dourdan, France (2008), CERN Yellow Reports: School Proceedings (2009).

[4] G. Klimpki et al., *A beam monitoring and validation system for continuous line scanning in proton therapy*, *Phys. Med. Biol.* **62** (2017) 6126.

[5] R.C. Webber, *Charged particle beam current monitoring tutorial*, *AIP Conf. Proc.* **333** (1995) 3.

[6] R. Dölling, *Profile, Current, and Halo Monitors of the PROSCAN Beam Lines*, *AIP Conf. Proc.* **732** (2004) 244.

[7] P. A. Duperrex, *Latest Diagnostic Electronics Development for the PROSCAN Proton Accelerator*, *AIP Conf. Proc.* **732** (2004) 268.

[8] R. Dölling, *Beam Diagnostics for Cyclotrons*, in *Cyclotrons 2010, Proceedings of 19th International Conference on Cyclotrons and their Applications*, Lanzhou, China (2010), pg. 344, http://accelconf.web.cern.ch/AccelConf/Cyclotrons2010.

[9] R. Dolling, *Ionisation chambers and secondary emission monitors at the PROSCAN beam lines*, *AIP Conf. Proc.* **868** (2006) 271.

[10] S. Srinivasan and P.-A. Duperrex, *Dielectric-Filled Reentrant Cavity Resonator as a Low-Intensity Proton Beam Diagnostic*, *Instruments* **2** (2018) 24.

[11] S. Srinivasan, P. Duperrex, and J. M. Schippers, *Beamline characterization of a dielectric-filled reentrant cavity resonator as beam current monitor for a medical cyclotron facility*, *Phys. Med.* **78** (2020) 101.

[12] R. Lorenz, *Cavity beam position monitors*, *AIP Conf. Proc.* **451** (1998) 53.

[13] S. Srinivasan, *Fourfold Dielectric-filled Reentrant Cavity BPM: Simulation and Measurement Summary*, zenodo (2021).

[14] S. Srinivasan, *Non-Interceptive Beam Current and Position Monitors for a Cyclotron Based Proton Therapy Facility*, University of Groningen, Groningen, The Netherlands (2021).

2022 JINST 17 P09013

[15] F. Gerigk, *Cavity types*, in *CAS — CERN Accelerator School: RF for accelerators*, Ebeltoft, Denmark (2010), pg. 277.

[16] S. Walston et al., *A metrology system for a high resolution cavity beam position monitor system*, *Nucl. Instrum. Meth. A* **728** (2013) 53.

[17] E. Jensen, *RF Cavity Design*, in *CERN Accelerator School: Advanced Accelerator Physics Course (CAS 2013)*, Trondheim, Norway (2013), pg. 405 [arXiv:1601.05230].

[18] A. Gerbershagen, A. Adelmann, R. Dölling, D. Meer, V. Rizzoglio and J.M. Schippers, *Simulations and measurements of proton beam energy spectrum after energy degradation*, in *IPAC 2017 — Proceedings of 8th International Particle Accelerator Conference*, Copenhagen, Denmark (2017), pg. 4740.

[19] F.J.M. Farley, *Optimum strategy for energy degraders and ionization cooling*, *Nucl. Instrum. Meth. A* **540** (2005) 235 [physics/0404072].

[20] V. Anferov, *Energy degrader optimization for medical beam lines*, *Nucl. Instrum. Meth. A* **496** (2003) 222.

[21] J. Petzoldt et al., *Characterization of the microbunch time structure of proton pencil beams at a clinical treatment facility*, *Phys. Med. Biol.* **61** (2016) 2432.

[22] R.E. Shafer, *Beam position monitoring*, *AIP Conf. Proc.* **212** (1990) 26.

[23] *Peek Technical Data Sheet*, www.amsler-frey.ch (2016).

[24] *Aluminum Oxide Ceramic Properties*, https://www.accuratus.com/alumox.html (2020).

[25] *ANSYS HFSS*, http://www.ansys.com/products/electronics/ansys-hfss/hfss-capabilities#cap2 (2017).

[26] F. Caspers, *RF engineering basic concepts: S-parameters*, *Cern Yellow Rep.* (2011), pg. 67 [arXiv:1201.2346].

[27] A. Gallo, A. Ghigo, F. Marcellini, M. Serio, B. Spataro and M. Zobov, *The transverse feedback kicker*, https://www.lnf.infn.it/acceleratori/dafne/NOTEDAFNE/CD/CD-5.pdf (1995).

[28] *Newport FCL Series Linear Stages User's Manual*, (2019).

[29] *FSH8 Spectrum Analyzer Operating Manual*, Munich, Germany (2020), https://www.rohde-schwarz.com/ca/manual/r-s-fsh4-8-13-20-operating-manual-manuals-gb1_78701-29159.html.

[30] *Radiocommunications in Switzerland*, www.bakom.admin.ch (2020).

[31] C. Ziomek and P. Corredoura, *Digital I/Q demodulator*, *Proc. IEEE Part. Accel. Conf.* **4** (1995) 2663.

[32] A. Patriarca et al., *Experimental Set-up for FLASH Proton Irradiation of Small Animals Using a Clinical System*, *Int. J. Radiat. Oncol. Biol. Phys.* **102** (2018) 619.

[33] R. Dolling, *Ionisation chambers and secondary emission monitors at the PROSCAN beam lines*, *AIP Conf. Proc.* **868** (2006) 271.

2022 JINST 17 P09013